Assessing the climate impact of the AHEAD multi-fuel blended wing body

Grewe, Volker; Bock, L.; Dahlmann, K.; Gierens, K.; Hüttenhofer, L.; Unterstrasser, S.; Gangoli Rao, Arvind; Bhat, Abhishek; Yin, Feijia; Reichelt, T.G.

DOI
10.1127/metz/2016/0758

Publication date
2017

Document Version
Final published version

Published in
Meteorologische Zeitschrift

Meteorologische Zeitschrift, PrePub DOI 10.1127/metz/2016/0758

Assessing the climate impact of the AHEAD multi-fuel blended wing body

Volker Grewe[1,2*], Lisa Bock[1], Ulrike Burkhardt[1], Katrin Dahlmann[1], Klaus Gierens[1], Ludwig Hüttenhofer[1], Simon Unterstrasser[1], Arvind Gangoli Rao[2], Abhishek Bhat[2], Feijia Yin[2], Thoralf G. Reichel[3], Oliver Paschereit[3] and Yeshayahou Levy[4]

[1]Deutsches Zentrum für Luft- und Raumfahrt, Institut für Physik der Atmosphäre, Oberpfaffenhofen, Germany
[2]Delft University of Technology, Aerospace Engineering, Delft, The Netherlands
[3]Chair of Fluid Dynamics, Hermann-Föttinger-Institut, Technische Universität Berlin, Berlin, Germany
[4]Israel Institute of Technology, Technion, Haifa, Israel

(Manuscript received November 18, 2015; in revised form June 16, 2016; accepted June 22, 2016)

Abstract

Air traffic is important to our society and guarantees mobility especially for long distances. Air traffic is also contributing to climate warming via emissions of CO_2 and various non-CO_2 effects, such as contrail-cirrus or increase in ozone concentrations. Here we investigate the climate impact of a future aircraft design, a multi fuel blended wing body (MF-BWB), conceptually designed within the EU-project AHEAD. We re-calculate the parameters for the contrail formation criterion, since this aircraft has very different characteristics compared to conventional technologies and show that contrail formation potentially already occurs at lower altitudes than for conventional aircraft. The geometry of the contrails, however, is similar to conventional aircraft, as detailed LES simulations show. The global contrail-cirrus coverage and related radiative forcing is investigated with a climate model including a contrail-cirrus parameterisation and shows an increase in contrail-cirrus radiative forcing compared to conventional technologies, if the number of emitted particles is equal to conventional technologies. However, there are strong indications that the AHEAD engines would have a substantial reduction in the emission of soot particles and there are strong indications that this leads to a substantial reduction in the contrail-cirrus radiative forcing. An overall climate impact assessment with a climate-chemistry response model shows that the climate impact is likely to be reduced by 20 % to 25 % compared to a future aircraft with conventional technologies. We further tested the sensitivity of this result with respect to different future scenarios for the use of bio fuels, improvements of the fuel efficiency for conventional aircraft and the impact of the number of emitted soot particles on the radiative forcing. Only the latter has the potential to significantly impact our findings and needs further investigation. Our findings show that the development of new and climate compatible aircraft designs requires the inclusion of climate impact assessments already at an early stage, i.e. pre-design level.

Keywords: AHEAD project, Multi fuel blended wing body, contrails, climate impact, air traffic

1 Introduction

Air traffic is a part of our mobility with an increasing rate in transport volume in the order of 5 % per year (Lee et al., 2010). Clean Sky, the European private public partnership (www.cleansky.eu), states that "Air transport's contribution to climate change represents 2 % of human-induced CO_2 emissions". Putting the focus from a carbon footprint to an ecological or climate footprint increases the importance of air traffic on climate change. Contrail-cirrus, atmospheric ozone, methane, water vapour, and particle concentrations are altered by aviation and add to the carbon dioxide induced aviation's contribution to climate change. Hence a 2 % contribution to carbon dioxide emissions turns into a roughly 5 % contribution to climate change (Lee et al., 2010). The European Commission whitepaper (EC, 2011a) clearly states that "transport is fundamental to our economy and society" and that it "is aiming at a competitive and resource efficient transport system" to contribute to "limiting climate change below 2 °C". Thus it implies for new aircraft developments to include climate impact assessments rather than evaluations of CO_2 emissions as currently frequently done, e.g. within Clean Sky.

Within the European project AHEAD (www.ahead-euproject.eu) new combustor technologies were investigated for use at a blended wing body (BWB). Two types of fuels are considered in series in two combustion chambers in order to reduce emissions (multi-fuel blended wing body, MF-BWB). In a first combustion chamber liquid hydrogen (LH2) or liquid natural gas (LNG), i.e. methane, is burnt to reduce the CO_2 emissions. A part of the emerging exhaust is inserted into the second combustor chamber, which is fueled with bio kerosene and burnt flameless in a water vapour

*Corresponding author: Volker Grewe, Institut für Physik der Atmosphäre, DLR-Oberpfaffenhofen, Münchener 20, 82234 Weßling, e-mail: volker.grewe@dlr.de

Table 1: Overview on the methods and models used in this study.

Model/Method	Description	Objective	Reference	Remarks
SAC	Schmidt-Appleman criterion	Condition for contrail formation	Schumann (1996)	Calculation of parameters required due to the use of two fuels
EULAG-LCM	EULerian and LAGrangian framework for solving the anelastic equations with a Lagrangian Cirrus Module	Characterisation of early contrail stage	Prusa et al. (2008); Sölch and Kärcher (2010)	Large-Eddy-Simulation including a Lagrangian tracking of ice crystals
ECHAM4-CCMod	ECHAM4 incl. Contrail-Cirrus Model	Estimate of contrail-cirrus impacts and sensitivities	Burkhardt and Kärcher (2009)	Climate model simulating interaction of cirrus and contrail-cirrus
ECHAM5-CCMod	ECHAM5 incl. updated Contrail-Cirrus Model	Estimate of soot reduction impact on contrail-cirrus RF	Bock (2014)	2-moment scheme for cirrus and contrails: ice mass and number density
AirClim	Air traffic Climate impact model	Estimate of overall climate impact	Grewe and Stenke (2008); Dahlmann et al. (2016)	Response model including effects from CO_2, NO_x, H_2O and contrail-cirrus
Climate objective	Detailed formulation of the underlying objective with regard to climate mitigation	Basis for the climate impact assessment	Grewe and Dahlmann (2015)	Defines implicitly climate metric, time horizon, fleet development, and a reference

rich and low oxygen environment reducing NO_x emissions. From the conceptual point a decrease in emissions is obvious, but the impact on climate via non-CO_2 effects is not obvious, since the impact also depends on the region where species are emitted (e.g., Grewe and Stenke, 2008; Frömming et al., 2012). Furthermore, it is crucial to consider the non-CO_2 effects as well, since the radiative forcing, e.g., of todays contrail-cirrus is larger than that of CO_2 ever since emitted by air traffic (Burkhardt and Kärcher, 2011). Here we exemplarily demonstrate the importance and need for the inclusion of such a climate assessment, already during the development of new technologies, which includes CO_2, contrail-cirrus, NO_x and water vapour effects. Section 2 will give an overview on the applied methods and the applied atmospheric models. Section 3 describes the AHEAD engine and aircraft including emissions on both engine and fleet basis. Section 4 shows results on the simulation of contrails for the AHEAD aircraft and Section 5 presents the potential of the AHEAD aircraft to reduce the overall climate impact relative to a conventional technology.

2 Methods

2.1 Overview

Table 1 provides an overview on the applied atmospheric models (also briefly described in the following sections) and methods. We first calculated the parameters for the contrail formation criterion (Schmidt-Appleman criterion) based on the use of two different fuels. We then performed Large-Eddy-Simulations (LES) to describe the contrail geometry and microphysical properties for the new and a reference aircraft (Section 2.2, EULAG model). In a third step, the probability of contrail formation at a given atmospheric state, the global coverage and radiative forcing (RF) of a fleet of AHEAD aircraft are calculated using a climate model which includes a contrail-cirrus parameterisation (Section 2.3, ECHAM4/5-CCMod). Results from this simulation are then used in a climate-chemistry response model (Section 2.4, AirClim) to estimate the overall climate impact of a fleet of AHEAD aircraft.

We concentrate on the contribution of the AHEAD technology to a reduction of the long-term temperature change. In other words we consider the question: “How much is the AHEAD technology reducing the long-term climate impact in comparison to a future conventional technology?". This defines well the climate objective (Table 1) and important implications of the overall climate assessment can be deduced (see also Tables 2, 3 and Grewe and Dahlmann (2015) for the procedure). We define a reference aircraft with approximately the same range (7,500 nm, roughly 14,000 km), the B787-800 (abbreviated as B787) and as a comparison also the B777-ER200 (B777), which comprise two different technology levels a newer and an older one, respectively. Since we address the contribution to a long-term climate impact, we need to consider a whole fleet. We regard a plausible fleet development: an entry into service (EIS) in 2050, a constant increase of the fleet size until 2075, reaching a certain market share, which stays constant after 2075. Since we regard an entry into service (EIS) for the AHEAD aircraft in 2050, we also add some future enhancements in fuel efficiency of 10 % for the refer-

Table 2: Basic assumptions for the AHEAD fleet scenario.

Scenario parameters	Value
Reference aircraft with year 2000 technology	B777-200ER
Reference aircraft with year 2014 technology	B787-8
Reference aircraft with year 2050 technology	B787-FUT
Entry into Service (EIS)	2050
Full fleet size	2075
Constant market share	2075-2150
Future fuel efficiency improvement (B7878-FUT)	10 %
Carbon neutral contribution by drop-in bio fuel	25 % (2050)
Number of city pairs	10
Annual flown reference distance for full fleet	5.4 10^8 km

ence aircraft (EC, 2011b; IATA, 2013), which we call B787-FUT and take an efficient reduction in CO_2 emissions of 25 % into account by using drop-in bio fuels. This defines a temporal evolution of the fleet with specific emission characteristics, i.e. an emission scenario, which will be described in more detail in Section 3. The emission scenario includes a spatial resolution based on characteristic 10 city pairs (Table 2). The long-term climate impact is then evaluated by calculating the global mean near surface temperature change associated with these fleet emissions for a 100 year time period starting from entry into service.

The climate impact assessment of this new aircraft requires some considerations with respect to contrail processes. These are presented in the following sections. Other effects arising from CO_2, H_2O, and NO_x emissions can be characterised by the emission strength and location and are analysed with the AirClim chemistry-climate response model without the need of any further enhancements (Section 2.4).

2.2 EULAG-LCM

We use the LES model EULAG (Prusa et al., 2008) together with the Lagrangian ice microphysics code LCM (Sölch and Kärcher, 2010) to perform high-resolution 3D numerical simulation of the early stage of the contrails from a MF-BWB aircraft. Recent contrail simulations with this code have been performed by Unterstrasser (2014). EULAG solves the anelastic approximation of the Navier-Stokes equations and LCM uses a particle-based approach for the ice microphysics. Except for a few modifications, the simulation setup of the MF-BWB contrail simulation is analogous to Unterstrasser (2014).

Adaptations are required, because the MF-BWB simulations are peculiar for the special geometry of the engines, which are located close to the centre of the aircraft, and for the ice and water content of the exhaust plume (where we use characteristics of the LH2 engines). We follow the contrail evolution over 5 minutes with time steps of $O(0.01\,\mathrm{s})$ and mesh sizes of $O(1\,\mathrm{m})$. The simulation starts at an assumed plume age of several seconds, that is, 5 to 10 spans behind the aircraft, when the microphysical process of ice formation is already terminated (about one wingspan behind the aircraft) and the roll-up process of the wing-tip vortices is in an advanced state.

For the flow field behind the MF-BWB, we use a pair of counter-rotating vortices in analogy to a conventional aircraft. The centres of the vortices have a separation distance of 55 m and their initial circulation Γ_0 is $550\,\mathrm{m^2 s^{-1}}$ (which is deduced from the typical weight, speed and span of the MF-BWB). For the initial exhaust distribution, we assume that the two initially separated jet plumes had expanded and merged into a rectangle of $20{\times}8\,\mathrm{m^2}$ which is filled homogeneously with ice crystals containing exactly the amount of emitted water vapour.

The total number of these ice crystals depends on the soot emission and we simply assume here that the kerosene burning produces soot at a typical rate of conventional engines with $2.8\,10^{14}$ ice crystals per kg of burned kerosene. Using these assumptions and consistent with the values of Table 6, we have an initial ice mass/number of $\mathcal{I}_0 = \mathcal{I}_{0,LH2} = 3\,10^{-2}\mathrm{kg\,m^{-1}}$ and $\mathcal{N}_0 = \mathcal{N}_{0,LH2} = 0.51\,10^{12}\,\mathrm{m^{-1}}$ (per metre of flight path). The ice crystal number is about one order of magnitude smaller than for a conventional aircraft of similar size, whereas the ice mass is twice as large (A340/B747: $\mathcal{N}_{0,conv} = 3.4\,10^{12}\,\mathrm{m^{-1}}$ and $\mathcal{I}_{0,conv} = 1.5\,10^{-2}\,\mathrm{kg\,m^{-1}}$).

In the vertical, both the vortex pair and the plume are centred on cruise altitude. For the atmospheric conditions we chose an ambient temperature of 217 K, a Brunt-Väisälä frequency of $1.15\,10^{-2}\,\mathrm{s^{-1}}$ and a relative humidity with respect to ice of 120 %. The latter is a moderate supersaturation value that guarantees that the contrail would be persistent, but natural cirrus formation via homogeneous freezing of ambient liquid aerosol droplets would not yet commence.

2.3 ECHAM4/5-CCMod

We study the effect of contrail-cirrus on climate using the German Community Climate Model ECHAM4-CCMod that was extended to simulate contrail cirrus as an independent cloud class consistent with the natural cloud scheme (Burkhardt and Kärcher, 2009). The frequency of ice supersaturation, which is the condition for contrail-cirrus persistence, is parameterised (Burkhardt et al., 2008). The following processes controlling contrail cirrus coverage and properties are parameterised:

1. contrail formation according to the Schmidt-Appleman criterion (see Section 4.1)
2. advection of contrails with the flow and persistence depending on ice supersaturation
3. contrail spreading proportional to the wind shear and vertical extent of the contrails
4. microphysical processes and optical properties as parameterised for natural clouds.

Table 3: Characteristics of the six aircraft types and respective fleets. Energy by kerosene means the contribution of kerosene to the propulsion. Fuel consumption equals kerosene consumption for conventional technologies and the sum of LH2 (LNG) and kerosene for the AHEAD-LH2 (AHEAD-LNG) aircraft. CO_2 emissions include a 25 % reduction for kerosene use due to biofuels (see Table 2). Pax abbreviates passenger.

	Units	B777	B787	B787-FUT	AHEAD-LH2-Min	AHEAD-LH2-Max	AHEAD-LNG
Technology Level	year	2000	2014	2050	2050	2050	2050
Passengers	number	300	225	225	300	300	300
Energy by kerosene	%	100	100	100	33	33	33
Kerosene mass	%	100	100	100	54	54	35
Flight level	hfeet	310–370	350–430	350–430	430	430	430
Fuel consumption	Tg/year	838	538	484	272	300	443
Pass. fuel cons.	kg/100 pax-km	2.79	2.39	2.15	0.91	1.00	1.48
CO_2-Emission	Tg/year	14.3	9.17	6.19	1.91	2.10	6.23
H_2O-Emission	Tg/year	5.68	3.64	3.27	7.02	7.72	4.67
NO_x-Emission	10^6 kg(NO_2) per year	73	34	31	13	14	9

The radiative impact of contrail-cirrus depends on the background cloudiness (natural clouds and contrail-cirrus). Therefore, we need to prescribe the emissions of a complete air traffic fleet in our model. In order to be able to isolate the effect of changing to AHEAD aircraft we replace all aircraft by AHEAD aircraft. We calculate the effect of contrail-cirrus taking into account the change in the Schmidt-Appleman criterion (Section 4.1) and an increase in the cruise altitude by 2000 m. Additionally, we performed a simulation without changes in cruise altitude and with small changes (700 m) for diagnostic purpose, i.e. to separate the effect of changing the SAC and changing the cruise altitude. The AERO2k air traffic scenario (Eyers et al., 2004) was employed for the base case simulation as well as for the parametric studies on the cruise altitude changes. Simulations over 10 years were carried out with ECHAM4-CCMod including online calculations of the stratosphere-adjusted radiative forcing (e.g. Hansen et al., 1997) as a measure for the radiative imbalance of the atmosphere due to contrail-cirrus.

Note that in these simulations we do not calculate explicitely any changes that may be due to changes in the soot number emissions as the latter are not known. Using LH2 or LNG in one of the combustors should lead to a significant reduction in soot number emissions. These are expected to lead to significant reductions in the initial ice crystal number (Kärcher and Yu, 2009; Kärcher et al., 2015) and therefore in contrail-cirrus radiative forcing (Zhang et al., 1999; Meerkötter et al., 1999). This effect is dependent on ambient temperatures. A decrease in temperature, as connected with an increase in flight level, leads to an increase in initial ice crystal number. Therefore, we refer to a recently updated model version ECHAM5-CCMod (Bock, 2014; Bock and Burkhardt, 2016), which includes not only the parameterisation of the contrail-cirrus ice mass but also the ice particle number densities. As the results of Bock (2014) indicate a substantial reduction in the RF of around 60 % if the soot emission number is globally reduced by 80 %, we consider this effect also for the AHEAD simulations (Section 5).

2.4 AirClim

The climate-chemistry response model AirClim (Grewe and Stenke, 2008; Dahlmann et al., revised) combines results of detailed climate-chemistry models, with emission data to obtain time series of RF and temperature changes caused by these emissions. These climate-chemistry model results describe the impact of a local emission on the radiation budget, e.g. the change in contrail-cirrus radiative forcing due to air traffic as resulting from the simulations described in Section 2.3, and eventually on the global mean near surface temperature. So far, the impact of CO_2, NO_x, H_2O emissions and flight distances on the atmosphere are taken into account via the climate agents CO_2, O_3, CH_4, primary mode ozone (PMO, i.e. the feedback of methane changes on ozone), H_2O, and contrail-cirrus.

All effects which are simulated with AirClim, except contrail-cirrus, can be described based on amount and location of emissions. The formation of contrails depend also on fuel and aircraft parameters. Therefore we adapted the model to be able to simulate the effects of the AHEAD fleet. The previously used response function between contrail-cirrus coverage (*CCCov*) and RF:

$$RF(lat) = CCCov \times 14.9 \frac{\mathrm{W}}{\mathrm{m}^2} \qquad (2.1)$$

was refined based on results of the ECHAM4-CCMod model.

The climate impact of contrail-cirrus in AirClim 2.0 was estimated based on a particular climate model simulation using a particular air traffic inventory. The application of AirClim to another aircraft inventory and changed contrail formation conditions are likely to result in discrepancies in radiative forcing as compared to the full climate model simulations. And hence four

Table 4: Results for the RF [mW m^{-2}] from contrail-cirrus of the AHEAD and conventional fleets for the standard and revised AirClim model version in comparison to the ECHAM4-CCMod model. Delta describes the relative difference [%] of the revised version AirClim 2.1 to the ECHAM4-CCMod results.

	AirClim 2.0 mW m^{-2}	AirClim 2.1 mW m^{-2}	ECHAM4-CCMod mW m^{-2}	Delta %
LH2	39.58	68.75	71.76	4.2
LNG	38.03	63.15	63.87	1.1
Conv.	34.16	38.63	38.94	0.8

discrepancies between the AirClim 2.0 and ECHAM4-CCMod results for the RF of the AHEAD versus the conventional aircraft were found and the response function refined accordingly. First the contrail-cirrus coverage is found to be larger by the a factor F, which equals the ratio of the overall propulsion efficiencies η, e.g. $F(\mathrm{LH2}) = \frac{\eta_{\mathrm{LH2}}}{\eta_{\mathrm{conventional}}}$. Second, a shift of the contrail coverage towards the equator was found, which is expressed by a latitude (lat, in °N) dependent function $f(lat) = 0.86 \cos\left(\frac{\pi\, lat}{50}\right) + 1.62$. Third, the RF from conventional aircraft show a latitude dependency, which has not been regarded yet: $h(lat) = 0.24 \cos\left(\frac{\pi\, lat}{23}\right) + 1.00$. And fourth, the AHEAD aircraft show additionally a further RF variation, which is expressed by: $g(lat) = 0.25 \sin\left(\frac{\pi\, |lat|}{42}\right) + 1.10$ (and $g(lat) = 1$ for conventional aircraft). These refinements then lead to the new RF response function in the revised model version AirClim 2.1:

$$RF(lat) = F \times f(lat) \times g(lat) \times h(lat) \times CCCov \times 14.9\, \frac{\mathrm{W}}{\mathrm{m}^2}, \quad (2.2)$$

which improve the agreement between AirClim and ECHAM4-CCMod (Table 4). Note that these refinements occur in addition to the changed Schmidt-Appleman criterion, which is incorporated in AirClim.

3 Engine, aircraft, and emissions

3.1 Engine and aircraft

We are considering a new combustion technology with a dual combustion chamber (Figure 1, top) mounted on a blended wing body (Figure 1, bottom), which is fully described in Rao et al. (2014). The engine requirements are (1) multi-fuel capability, (2) low emissions of NO_x and particles, (3) low installation penalty, and (4) capable for ingestion of the aircraft's boundary layer, which the regarded engine fulfills (Rao et al., 2014). The engine is designed so that 70 % of the energy is provided by the LNG and LH2 combustion, respectively and 30 % by bio kerosene (Table 3).

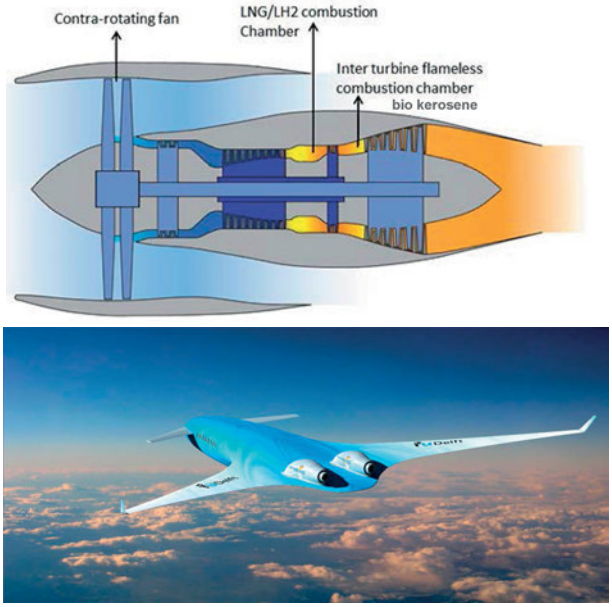

Figure 1: Top: Sketch of the AHEAD engine (cross section). The two combustion rings for LH2/LNG and bio fuel (kerosene) combustion are marked. Bottom: Drawing of the AHEAD MF-BWB.

In order to have the fuel storage possibilities and an improved lift to drag ratio a blended wing body was chosen as an adequate airframe (Figure 1, bottom). Table 3 describes some characteristics of the 2-engine AHEAD aircraft, such as a capacity of 300 passengers, a cruising at flight level FL 430 (around 13 km) and a range of 14,000 km, which corresponds to around 7,500 nm. An iterative procedure is used to design the aircraft, which includes sizing, weight, stability and control, propulsion, structures, and a performance analysis (Roskam, 1997). A first design optimisation was performed to achieve optimal lift to drag ratio during cruise. However, a first climate impact assessment gave evidence to a large climate impact due to water vapour emissions at high cruise altitudes (see also Grewe et al., 2007; Grewe et al., 2010). Hence, the cruise altitude was reduced to flight level 430, achieving a lift to drag ratio of about 25. The LH2 storage requires a large volume, which could impose some drag and weight penalties on the AHEAD aircraft. Since we did not investigate this effect in detail we consider two extreme situations, covering a wide range of possible aircraft dimensions: A minimum case (LH2-Min), where no changes in the aircraft design are necessary for LH2 storages and a maximum case with increased aircraft dimensions and weight (LH2-Max).

3.2 Emissions

The emission index of NO_x for the first and second combustor stage is calculated based on NO_x recordings obtained from atmospheric combustor experiments. Both test rigs allow establishing the same temperature boundary conditions with respect to the calculated adiabatic flame temperature T_{ad} as in the engine during cruise

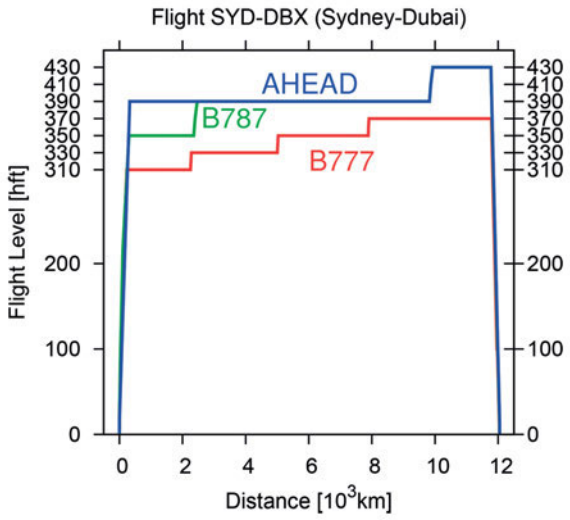

Figure 2: Flight profiles (trajectories) for the B777, B787, and the AHEAD aircraft on the route Sydney to Dubai.

(T_{ad}^{cruise} = 1850 K). Operating at atmospheric instead of elevated pressures is justified by the findings of Leonhard and Stegmeier (1994).

For the first stage, the LH2/LNG combustor, an unprecedented combustor design, was developed by Reichel et al. (2015a), capable of burning both fuel types, LH2 and LNG. The lean premixed combustor design applies an additional non-swirling axial air jet in a swirl-stabilized combustor environment in order to maximise the operational range. By this means the design is shown to allow for safe, low-emission operation even in case of a high-reactivity fuel like hydrogen.

The recorded data show nitrogen oxide emissions well below 10 ppm, which translates to 3 g(NO_2) per kg fuel, for the AHEAD-LH2 and AHEAD-LNG aircraft (Reichel et al., 2015b).

Flameless combustion is used in the second chamber burning bio kerosene, i.e. a part of the exhaust of the first combustion chamber, which is humid, hot and with low oxygen content, is redirected into the second combustion chamber in which kerosene is injected. The mixture is rotating in the relatively large combustion chamber and burning in a large volume without a visible flame. A CFD calculation including the chemical code CHEMKIN (Kee et al., 2006) showed very low NO_x emissions of 0.5 ppm (Levy et al., 2014), i.e. negligible in comparison to the emissions from the first combustion chamber. Experimental data of a designed combustor model largely confirmed the results.

3.3 Fleet emissions

In order to obtain a fleet emission inventory, we selected 10 appropriate and representative city-pairs for long-distance flights. Flight trajectories are then calculated for all 6 aircraft types (Table 3). An example is given in Figure 2 showing the different flight altitudes for the flight Sydney to Dubai. Note that the fuel types differ in terms of combustion energy. So that the annual fuel consumption varies between 272 Tg and 838 Tg and the fuel per passenger-km varies between 0.9 kg per 100 passenger-km and 2.8 kg per 100 passenger-km (Table 3). The calculation of the annual CO_2 emission includes the use of bio fuels for the future (Table 2) and ranges between 1.9 Tg per year for the AHEAD-LH2 fleet and 14 Tg per year for the B777. Note that the comparison mixes different technology levels. For the same technology level (2050) the conventional technology and the AHEAD-LNG technology emits approximately the same amount of CO_2, whereas the AHEAD-LH2 fleet emits more water vapour. Note that we assume here that the production of LH2 can be achieved carbon neutrally. Nitrogen oxide emissions are reduced from 73 10^6 kg(NO_2)/year to 9 10^6 kg(NO_2)/year, i.e. roughly a 90 % emission reduction.

For multi fuel use, the normal emission index is meaningless, therefore we provide annual emissions (Table 3), which clearly show the reduced CO_2 and NO_x emissions for the AHEAD technologies in comparison to the future conventional technology. However, water vapour emissions are increased.

The regional distributions of H_2O and NO_x emissions are presented in Figure 3, showing that the selected 10 city pairs cover a representative area of the globe, with a maximum in northern mid latitudes (top). The vertical distribution (bottom) reflects the step climb shown in Figure 2 with a large fraction of the H_2O emissions of the AHEAD fleet deposited at flight level 430. The temporal evolution of the emission of aviation follows the IPCC FA1 scenario.

4 Contrails

In this section, we discuss in detail the contrail formation and contrail properties of the AHEAD aircraft in comparison to a conventional aircraft by using a modelling tool suite, which is described in Section 2 and Table 1. It is important to note that the detailed work on contrails and also some preliminary climate impact assessments (not shown) was performed in parallel to the work on the aircraft-engine design. This had on the one hand the great advantage that initial findings on the climate impact from, e.g., contrails and water vapour fed back to the aircraft/engine design. On the other hand the detailed studies were performed with preliminary emission data that differ from the final emission data presented in Section 3.3. However, Section 4 shows more principal results, which are less affected by the specific fleet layout. The overall climate impact assessment in Section 5 is, however, based consistently on the calculated fleet emissions in Section 3.3 and takes into account main results from this Section.

4.1 Contrail formation

The Schmidt-Appleman theory (Schmidt, 1941; Appleman, 1953; Schumann, 1996) states that a contrail

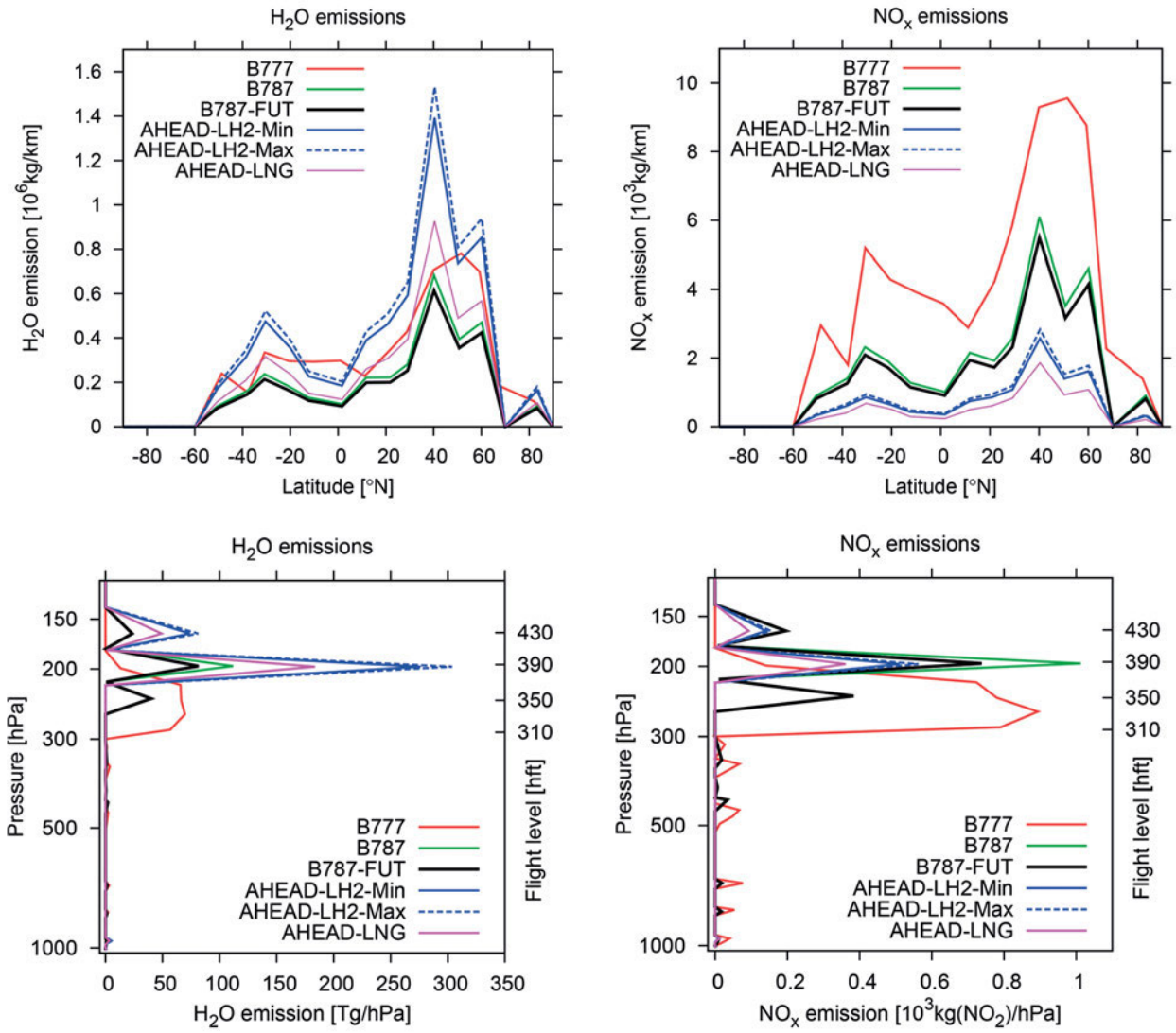

Figure 3: Fleet emission for the B777, B787, and the AHEAD aircraft for H_2O (left) and NO_x (right). The units are given in mass (kg) per distance latitude (km) and per pressure-altitude (hPa), respectively. The integral gives the total annual emission.

will form when the exhaust-air mixture in the expanding plume reaches water-saturation. The phase diagram (Figure 4) shows possible mixing trajectories: They start well outside the figure at high temperature and high water vapour pressure of the exhaust gas. Mixing with ambient air moves the mixture's phase-point down along a straight line which here touches the saturation curve for liquid water. Eventually the mixture approaches asymptotically the final point of the trajectory, which is solely given by the ambient temperature and water vapour pressure (not shown). A contrail will form if the mixing trajectory is tangential to the water vapour saturation curve or crosses it, i.e. trespasses into the water supersaturated regime. Then tiny droplets form by condensation (with the aid of mainly emitted soot particles that serve as condensation nuclei or abundant ambient particles) and they freeze quickly at temperatures below the supercooling limit of water, around −38 °C. The slope G of the mixing trajectory, the ambient temperature and the water vapour pressure are determining whether a contrail will form or not. The slope depends on air pressure, fuel and aircraft properties. The expression for G can be derived by an application of fundamental physical laws to the motion of an aircraft, namely the conservation of energy and linear momentum:

$$G = \frac{c_p p}{\epsilon} \frac{EI_{\mathrm{H_2O}}}{Q(1-\eta)}, \tag{4.1}$$

where c_p is the specific heat of air at constant pressure, and ϵ is the ratio of the molar masses of water and air. The slope G, depends furthermore on ambient pressure p, fuel properties, such as the emission of water vapour per kilogram fuel burnt, EI_{H_2O} and heat energy per kilogram fuel burnt, Q, and on the overall propulsion efficiency, η. The larger G, the higher is the maximum temperature at which a contrail can form. This maximum is marked by the tangential point of the mixing trajectory with the water saturation curve. In Figure 4 we show three tangential mixing trajectories, one for a conventional aircraft (driven by kerosene only with an over-

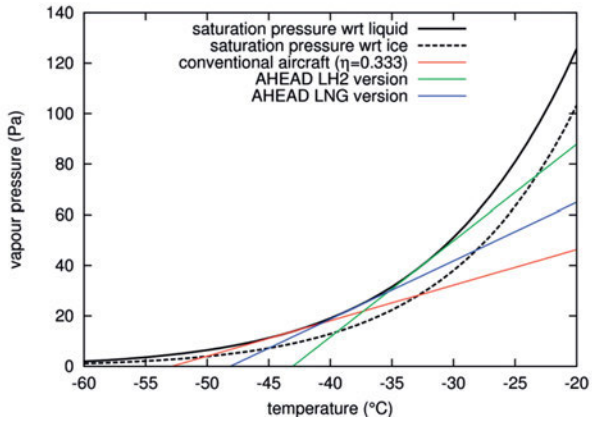

Figure 4: Water vapour pressure vs. temperature phase diagram representing thermodynamics of contrail formation for a conventional aircraft with overall propulsion efficiency of 0.333 (red line) and for two versions of an AHEAD aircraft LH2 (green line) and LNG (blue line). The two black curves are the saturation vapour pressure curves for water, the one with respect to liquid supercooled water (solid) and the one with respect to ice (dashed). The red, green and blue lines represent the temporal evolution of a mixture of engine exhaust gas with ever increasing amounts of ambient atmospheric air under threshold conditions, i.e. conditions that would just allow formation of a contrail (the lines are tangent to the saturation line with respect to liquid water). Phase points to the right of the mixing lines represent atmospheric states where contrail cannot form.

all propulsion efficiency of 0.333), and one for AHEAD-LH2 and LNG versions, respectively. (Details on the calculation of the slopes for the different aircraft are given in the appendix). The AHEAD aircraft (green and purple lines) form contrails at considerable higher temperatures than conventional aircraft (red line), mainly because of the enhanced emission index of water. As temperature generally decreases with altitude in the troposphere, higher contrail formation threshold temperatures can be translated into lower altitudes at which contrails can be formed. Here one has to consider that the condensed droplets must freeze to form a contrail. For pure water and droplets including poor freezing nuclei, such as aircraft soot, this requires temperatures below −38 °C. A climate impact of contrails is only present, once a contrail is persistent, i.e. long-living and extending into so-called contrail-cirrus (see below). The thermodynamic condition for this is that the ambient water vapour partial pressure reaches or exceeds ice saturation (dashed curve in Figure 4). The three threshold mixing trajectories in Figure 4 reach ice saturation (after first touching water saturation) at different temperatures.

4.2 Early contrail stage

During the first minutes after their formation, contrails strongly interact with the trailing wake vortices. On the one hand, this leads to a strong vertical expansion (contrail depths of more than 500 m are possible). On the other hand, adiabatic heating in the downward moving vortex system can lead to a substantial loss of ice crystals. Both processes affect the properties of the evolving contrail-cirrus (Unterstrasser and Gierens, 2010; Unterstrasser and Görsch, 2014).

Three cases are compared to allow a better justification of the environmental benefit of the MF-BWB in terms of contrail formation and their climate impact. These are (1) the MF-BWB with the LH2 engines, (2) a standard aircraft (A340/B747 type), and (3) a hypothetical aircraft with MF-BWB geometry but with standard kerosene combustion. We assume the same flight altitude for these three cases to isolate the effect of the airframe and fuel. All three simulations start with similar wake vortex characteristics (i.e. initial circulation and vortex separation), as the wing span, aircraft weight and speed are similar. Then the descent speed and decay of the vortex system are similar. Figure 5 (top) shows vertical ice mass profiles after 5 minutes (at an age when the wake vortices have already dissolved). The profiles are similar for all three cases. We conclude that differences in the initial ice mass $\mathcal{I}_0$ are of minor importance for the later ice mass evolution. This is due to the fact that the total ice mass increases (see Figure 5, mid), especially ice crystals in the secondary wake around the original contrail formation altitude at $z = 0$ m (cruise altitude) take up excess water vapour from the environment. The contribution of the initial water vapour emission to the total contrail mass becomes less and less. Initially, the majority of ice crystals is entrained into the vortex system and transported downwards. During the descent some ice crystals get detrained and form a curtain between the primary wake (i.e. the exhaust trapped within the vortices) and the original formation altitude. Eventually, the vortices break up and much material rises back due to buoyancy. The simulations suggest that these entrainment/detrainment effects are barely affected by the initial spatial exhaust distribution. This result is in line with previous sensitivity studies varying the initial distributions for conventional aircraft geometries (Huebsch and Lewellen, 2006; Unterstrasser and Görsch, 2014; Unterstrasser et al., 2014). Nevertheless, this rather weak sensitivity is unexpected, as the initial differences examined here are larger than in the previous studies.

Figure 5c shows the temporal evolution of ice crystal number. We note that the difference between the solid and the dashed line is much smaller than the difference of these with the dotted line. This shows that the contrail microphysical properties depend stronger on the composition of the exhaust (water and soot particles) than on the aircraft geometry (wing shape and position of the engines). In all cases there is some crystal loss due to sublimation in the downward traveling vortex pair, but the fraction of crystals that gets lost is larger in the two cases with a conventional engine (35 % vs. 5 % for the LH2 engine). The crystals are initially smaller, as the ratio $\mathcal{I}_0$ to $\mathcal{N}_0$ is smaller for a conventional engine, and they sublimate more easily than the bigger crystals of the LH2 contrail. After a few minutes the LH2 contrail

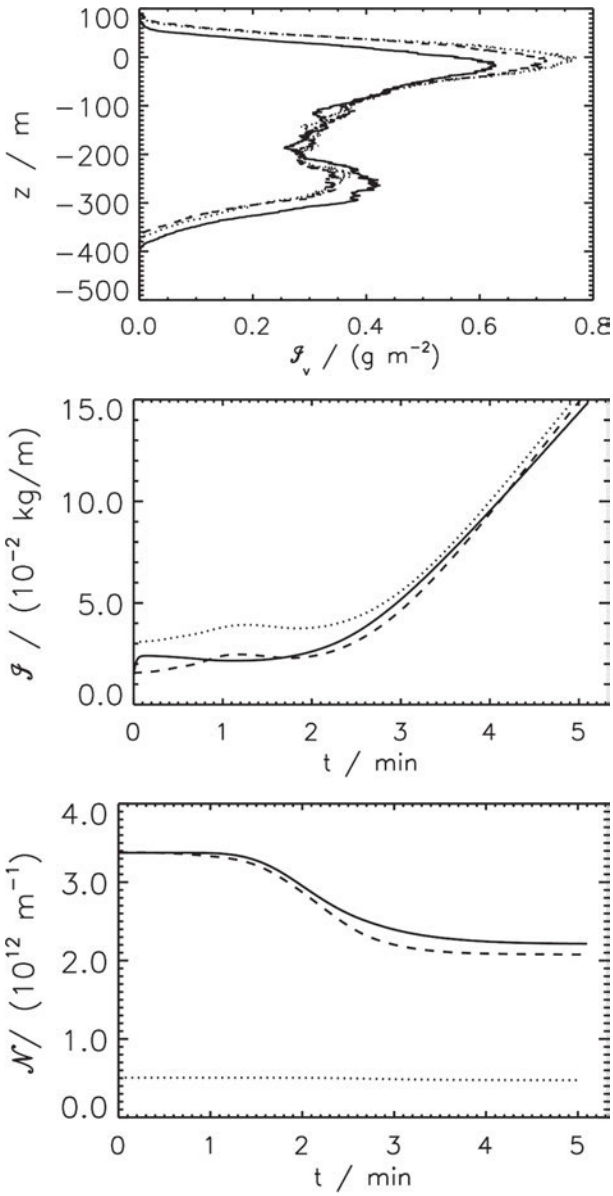

Figure 5: Top: Vertical profile of ice crystal mass after 5 minutes (i.e. after wake vortex break up). Middle and Bottom: Temporal evolution of ice crystal mass $\mathcal{I}$ and number $\mathcal{N}$, respectively. Three types of aircraft are depicted with different line styles: Dotted (MF-BWB geometry + LH2 engine), solid (B747/A340 + conventional engine), dashed (MF-BWB geometry + conventional engine)

contains 4 times fewer ice crystals than the conventional aircraft, which is less than at the beginning, where there were 6.7 times fewer ice crystals. Larger and less ice crystals as in the MF-BWB case imply (1) smaller optical thickness of the contrail and (2) larger crystal fall speeds and thus (3) shorter lifetime than in the cases with conventional engines. Therefore, for the here assumed number emission index of soot particles and in a direct comparison (same meteorology for both aircraft), the contrail climate impact of MF-BWB aircraft is expected to be smaller than that of conventional aircraft. The impact of different cruise levels (see Figure 2) and different fuels on the radiative forcing is investigated in the next Section.

4.3 Global contrail-cirrus

Figure 6 shows the change in the contrail formation probability due to the change in the Schmidt-Appleman criterion (see also Section 4.1) at 250 hPa and 300 hPa, the change in contrail-cirrus coverage and the radiative forcing caused by the replacement of a whole fleet of conventional aircraft by the AHEAD-LH2 aircraft including an upward shift of air traffic by 2000 m. It shows large increases of the contrail formation probability particularly in the tropics and subtropics that are mostly larger at lower levels (Figure 6a,b). In those areas at the main air traffic levels and below, contrail formation is limited by the Schmidt-Appleman criterion for conventional aircraft. Above 230 hPa contrail formation probability does not change significantly since at this altitude the Schmidt-Appleman criterion is usually fulfilled, but contrail persistence is limited by ice supersaturation frequency. The increase in the contrail formation probability is mainly due to the increase in water vapour emissions when considering the AHEAD-LH2 aircraft (see also Table 3). In the extra tropics, contrail formation conditions at the main flight levels are such that whenever tropospheric air is ice supersaturated contrails can usually form. Therefore, changing to an AHEAD-LH2 aircraft introduces only slight changes in the formation conditions in the extra tropics. The change in the contrail formation conditions alone induces an increase in the contrail-cirrus coverage (Figure 6c) and radiative forcing (Figure 6d) that is largest in the areas of maximum air traffic, over Northern America, Europe and Southeast Asia. The change over Southeast Asia is as large as over the main air traffic areas due to the fact that the formation conditions are changing much more strongly. The higher cruise altitude leads in the extra-tropics to a shift of the aircraft into the stratosphere where contrails cannot persist due to the low relative humidity and therefore to a decreased contrail-cirrus cover. In the tropics and subtropics the higher cruise altitude leads to an increase of air traffic in the upper troposphere and therefore to increased contrail-cirrus cover. Overall the change in formation conditions and the increase in cruise altitude lead to an increased contrail-cirrus cover over the main air traffic areas and over the tropics (Figure 6c). Contrail-cirrus radiative forcing is reduced in the extra tropics due to the higher cruise altitude and otherwise, mainly over the eastern USA and Southeast Asia, increased (Figure 6d). Overall, contrail-cirrus radiative forcing is increased by 50 %, when switching the whole air traffic fleet to AHEAD-LH2 technology and moving air traffic up by 2 km. Note that a mere shift of air traffic from flight level 370 to 380 would have led to a decrease of contrail-cirrus radiative forcing in the extra-tropics, since these flight would occure more frequently in the dry lower-most stratosphere. However, the additional shift of air traffic from lower levels into the upper troposphere compensated this effect. Note also that changes in soot number emissions are not regarded here (see discussion below).

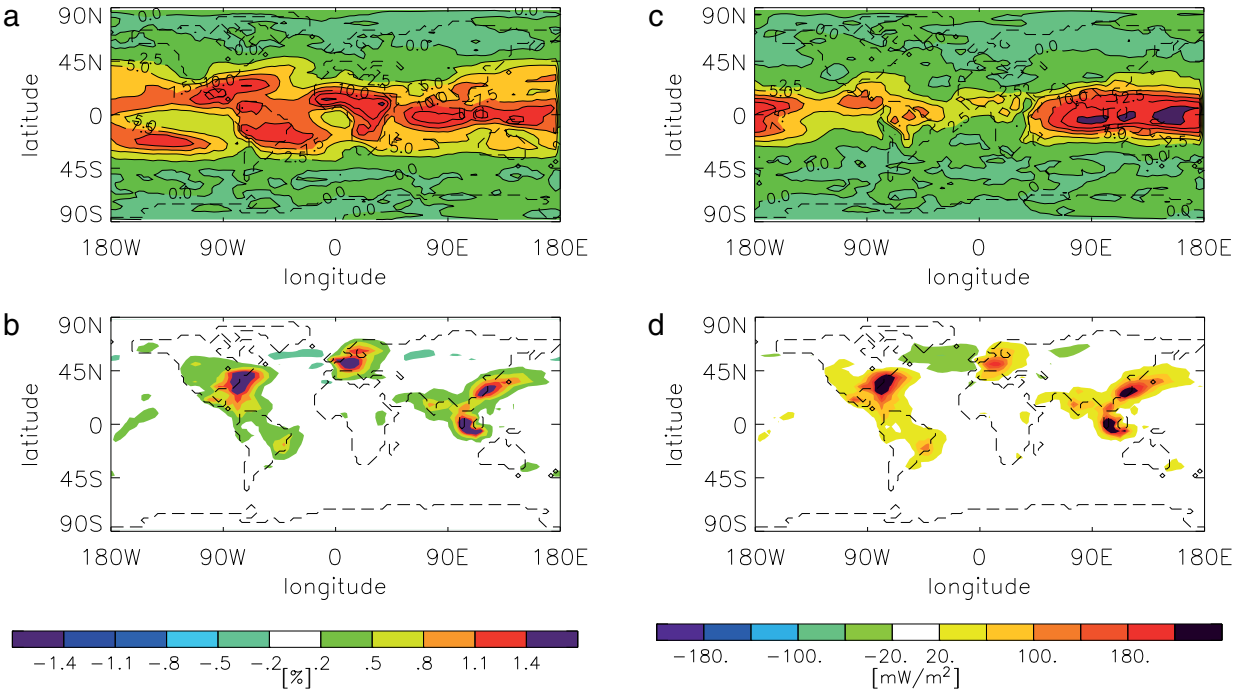

Figure 6: Change in contrail formation probability [%, percentage point] at 300 hPa (a) and 250 hPa (b) and change in contrail-cirrus coverage [%, percentage point] (c) and radiative forcing [mW m^{-2}] (d). The calculations include an increase of the cruise altitude and a change in the contrail formation conditions resulting from the replacement of conventional aircraft by AHEAD-LH2 aircraft (see text for more details). (a) and (b) have isolines every 2.5 % (dark green: below 2.5 %, light green–orange: 2.5 % to 7.5 %, red: above 7.5 %).

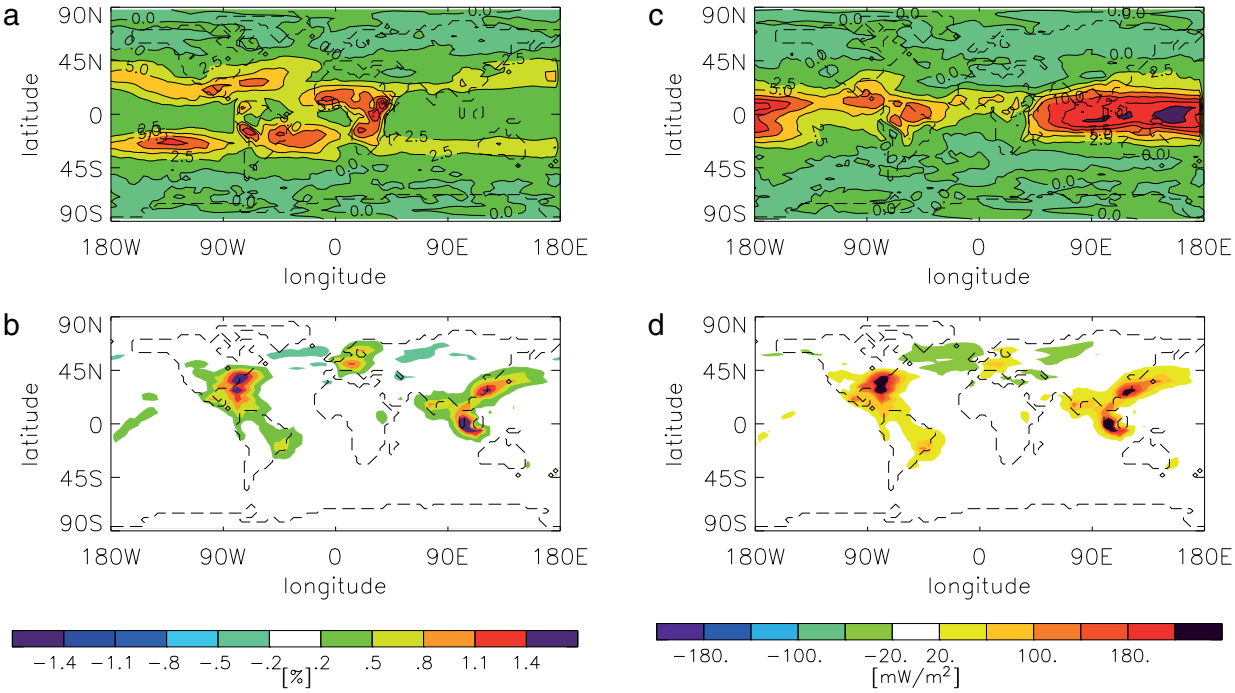

Figure 7: Same as Figure 6, but for the AHEAD-LNG aircraft.

Switching to the AHEAD-LNG aircraft and moving flight levels upwards is connected with very slight decreases in contrail-cirrus coverage and radiative forcing in the extra tropics and with increases in the tropics and sub tropics (Figure 7c,d). The change is hence similar to those of the AHEAD-LH2 aircraft (Figure 6c,d). The change in the formation probability at 300 hPa is smaller than for the AHEAD-LH2 aircraft. Changes in contrail-cirrus coverage and radiative forcing for the AHEAD-LNG aircraft are very similar to changes for AHEAD-LH2 aircraft, but slightly smaller (Figure 7c,d). Figure 8 summarises the results regarding the change in contrail-cirrus radiative forcing due to changes in the flight level and changes in the contrail formation probability caused

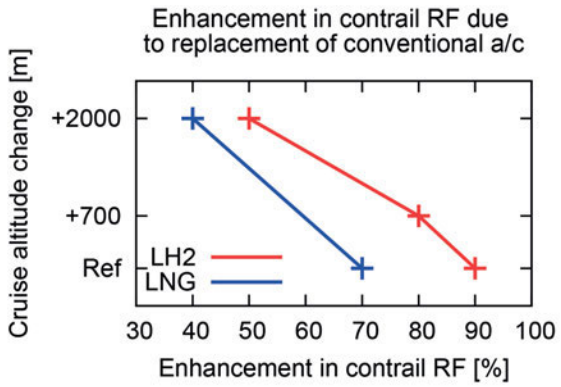

Figure 8: Altitude dependency of the enhancement in the contrail-cirrus radiative forcing due to a replacement of conventional aircraft by AHEAD-LH2 (red line) and AHEAD-LNG (blue line) aircraft. Changes in soot emissions are not regarded here.

by the emissions of the AHEAD-LH2 and AHEAD-LNG aircraft. Contrail-cirrus radiative forcing is larger by approximately 40 % for the AHEAD-LNG aircraft due to the change in the contrail formation probability and the upwards shift of air traffic.

A decrease in soot number emissions that is likely to be connected with replacing conventional aircraft by the AHEAD-LH2 and also AHEAD-LNG aircraft would be expected to lead to a decrease in initial ice crystal concentration on average, depending on the atmospheric state (Kärcher and Yu, 2009; Kärcher et al., 2015) and likely to a decrease in contrail-cirrus coverage and radiative forcing due to changes in the microphysical and optical properties and the associated shortening of the lifetime of contrail-cirrus (Bock and Burkhardt, 2016), when keeping the flight level unchanged. Based on this study, we conservatively assume a reduction of the RF by 40 % for a reduction in the soot number densities of 80 % and analyse the impact of this estimate in parametric sensitivity studies in Section 5.

5 Climate impact

In this Section, we investigate how much the introduction of the AHEAD aircraft reduces the long-term climate impact in relation to future conventional technology (see also Section 2.1). The fleets, as described in Section 3.3, are evaluated with the climate-chemistry response model AirClim (Section 2.4) with respect to the impact of CO_2, NO_x and water vapour emissions on the global-mean near-surface temperature change via the climate agents CO_2, O_3, CH_4, PMO, H_2O, and contrail-cirrus. Figure 9 shows the temporal evolution of this temperature change for the reference configuration B787-FUT (top) as well as the AHEAD fleets. Ozone changes and contrail-cirrus contribute most to the induced temperature increase for the B787-FUT, whereas contrails, water vapour, and ozone changes are important for the AHEAD technologies.

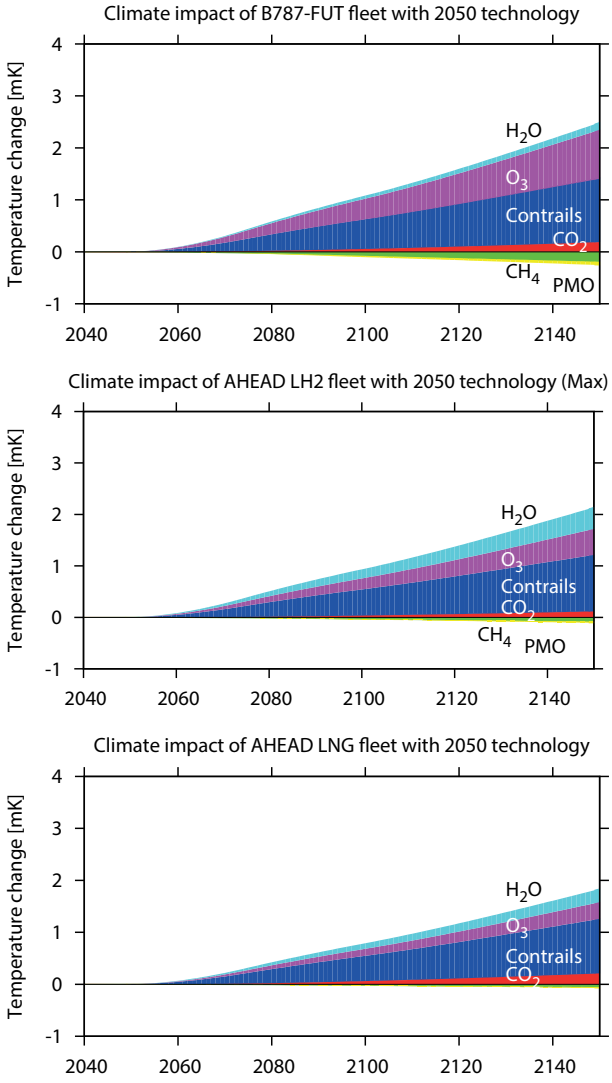

Figure 9: Temperature change [mK] induced by the B787-FUT (top), AHEAD-LH2-Max (mid), and AHEAD-LNG (bottom) fleet. Individual contributions are marked in color: H_2: light blue, O_3: magenta, contrail-cirrus: blue, CO_2: red, CH_4: green, and PMO: yellow.

Figure 10 (left) summarises the results on the climate impact as a change in the average temperature response over 100 years after introducing the fleet (ATR100). A clear improvement of the fleet's climate impact from the B777 to the B787 and the future technology B787-FUT is simulated, which is basically achieved by CO_2 and NO_x emission reductions. However, the higher cruise altitude of the B787 causes more (less) contrail formation in the tropics (mid-latitudes) with an overall increase in the contrail-cirrus RF and temperature change. The AHEAD technologies show a large reduction of the climate impact from NO_x emissions in the range of 15 % to 20 % and from contrail-cirrus in the order of 5 % to 10 % relative to the future conventional technology. Since the AHEAD aircraft has similar flight altitudes compared to B787 and B787-FUT, these reductions mainly arise from the low NO_x and soot emissions, respectively. The large water vapour emissions of the AHEAD technologies (see Table 3) compensate the climate impact reduc-

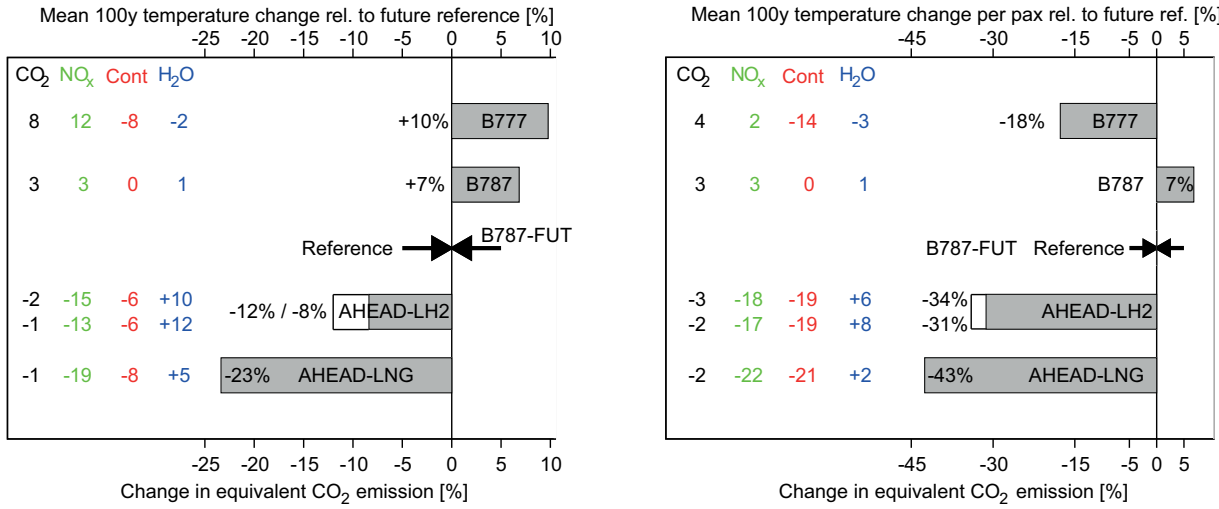

Figure 10: Left: Change in the average temperature response during 2051 to 2150 (ATR100) for the fleets of the different aircraft configurations relative to the reference configuration B787-FUT. The relative change in ATR100 equals the change in equivalent CO_2 emissions if ATR100 is used as the conversion factor for non-CO_2 effects. The contributions of CO_2 (black), NO_x (as a sum of O_3, CH_4, and PMO; green), contrail-cirrus (red), and H_2O (blue) are added as numbers on the left of the individual figures. Right: as left but relative to the same passenger-km.

tion by NO_x and contrail-cirrus significantly (roughly 5 % to 10 % of the climate impact of the reference). The high cruise altitude leads to larger residence time of the even larger amounts of emitted water vapour of the AHEAD aircraft compared to the conventional aircraft, which is in agreement with earlier studies (Grewe and Stenke, 2008; Grewe et al., 2010). The AHEAD-LNG version is even better, mainly because of lower water vapour and NO_x emissions (see also Table 3).

It is important to mention that the B787 has a lower passenger capacity than B777 and the AHEAD aircraft. Hence although the considered fleets have identical flight distances, the transport volume in terms of passenger kilometres differ by 33 %. In Figure 10 (right) we have considered this effect and compare the results with respect to the same transport volume. In this case, the climate impact of the reference (B787-FUT) is increased in comparison to the AHEAD aircraft configurations. Hence the climate impact reductions are even larger and increase from around 10 % to 25 % for the AHEAD fleets to roughly 30 % to 45 %.

The calculation of the future climate impact includes a couple of assumptions, which we discuss in the following (Table 5). We assumed for our climate impact calculation a 40 % reduction of the contrail-cirrus radiative forcing due to the reduced soot emission (see Section 2.3), which we regard as a conservative estimate. We tested a range of reduction factors from 0 % (i.e. no reduction) to 60 % (Table 5). Clearly this parameter largely affects the results. Assuming no impact of the reduced soot emissions (0 %), would even lead to opposite effects, the AHEAD technology would be worse than conventional. On the other hand, an even stronger impact of the reduced soot particle emissions (60 % reduction of the RF) leads to 25 % and to 40 % reduction of the climate impact of the AHEAD fleet.

Table 5: Average temperature response of the AHEAD fleet relative to the future conventional fleet [%] for variations in three parameters: Reduction of the contrail-cirrus RF due to reduced number of soot particles (soot effect), the effective reduction in CO_2 emissions due to the use of bio fuels, and the future increase in fuel efficiency for conventional technologies (see also Table 2). Note that the use of bio fuels refers to the conventional and AHEAD technologies.

Varied parameter	base	sens.	AHEAD LNG	AHEAD LH2-Min
Base value	–	–	−23	−8
soot effect	40 %	0 %	26	10
	40 %	20 %	−7	9
	40 %	60 %	−40	−24
bio fuel	25 %	50 %	−24	−7
	25 %	0 %	−23	−10
fuel efficiency	10 %	30 %	−15	1

A further uncertainty in the scenario definition is the amount of bio fuel used in future and the sustainability of the bio fuel production. In the base case we assumed a 25 % effective CO_2 reduction by bio fuels. A variation of this number to 0 % and 50 % changes the numbers only slightly, mainly for two reasons. First the fuel efficiency already reduced the impact of CO_2 from the B787 to B787-FUT. Further, the assumed evolution of the fleet reinforces the short-lived compounds more than the long-lived, such as CO_2. Further, we assumed an increase in fuel efficiency of the engine and conventional aircraft of 10 %. If a 30 % increase in fuel efficiency of the conventional technology could be achieved, then the AHEAD-LNG aircraft becomes only slightly (15 %) better than the conventional technology. However, this implicitly includes that these efficiencies cannot be used by the AHEAD aircraft (e.g. lighter materials).

6 Conclusion

We investigated the climate impact of a fleet of a multi-fuel blended wing body in comparison to a future conventional technology. The AHEAD aircraft is designed with engines having 2 combustion chambers fueled with either liquid hydrogen (LH2) or liquid natural gas (LNG) in the first combustion chamber and bio kerosene in the second. The AHEAD aircraft has a larger overall propulsion efficiency, larger water vapour emission index and the fuel mix has a larger specific heat content than the reference aircraft, which leads to a larger probability in the contrail formation. The layer where contrails can form starts at a lower altitude especially in the tropics. The shape and geometry of the contrails is not significantly affected, which was shown by LES simulations. The emission index of soot particles and the related effect on the contrail-cirrus optical properties have not been investigated in detail. However, there are strong indications that both the number of emitted soot particles and the effect on RF are significantly reduced for the AHEAD aircraft. To cover this effect, we started with detailed simulations without any changes in the number of emitted soot particles. In this case, the global contrail coverage and radiative forcing increases by 40 % and 50 % for the LNG and LH2 AHEAD aircraft, respectively. Simulations with a 80 % reduction in the number of soot particles (Bock, 2014) showed a 60 % reduction in the RF. Based on this first climate model study (Bock, 2014) we conservatively assumed a 40 % reduction in the radiative forcing of contrail-cirrus caused by the lower optical thickness and a shorter lifetime of the AHEAD contrail-cirrus compared to conventional technologies and varied this parameter in the range of 0 % to 60 % in a sensitivity analysis of the overall climate impact assessment. For this climate impact assessment, we took all relevant climate agents, i.e. CO_2, O_3, CH_4, PMO (latter three arising from NO_x emissions), H_2O, and contrail-cirrus into account. The results show that the AHEAD-LNG version significantly reduces the climate warming (about 20 to 25 %) in comparison to conventional technologies, whereas the LH2 version has a lower reduction potential. A sensitivity analysis showed that the results are robust against changes in the amount of bio fuel. Significantly larger increases in fuel efficiencies of 30 % for the future conventional aircraft than assumed here (10 %) would reduce the climate impact reduction of the AHEAD-LNG version to around 15 %, still having a lower climate impact than the conventional technology. The results crucially depend on the number of emitted soot particles for the AHEAD aircraft and on the impact of the soot emission index on the contrail properties, which still are under investigation.

It is important to note that only a frequent iteration between engine design, aircraft design and climate impact analysis ensured a climate compatible new design, since a first version had a low CO_2 and NO_x emission, but the cruise altitude was higher, which made the water vapour emissions more important for climate change, since the residence times of water vapour in the lower stratosphere are significantly higher than in the tropopause region. Clearly, a CO_2 reduction is important, but a climate impact reduction requires addressing also contrail-cirrus, water vapour and NO_x emissions. As a result of the close cooperation between the disciplines, we found that the AHEAD aircraft fueled by LNG and bio kerosene, flying at FL 430, represents an adequate technology to reduce the climate impact and equivalent CO_2 emissions.

Acknowledgments

The research leading to these results has received funding from the European Union Seventh Framework Programme (FP7/2007-2013) under grant agreement No. "284636" – the AHEAD project. The authors would like to acknowledge the support of all the partners of this project. The EULAG-LCM and the ECHAM4/5-CCMod model simulations were performed at the German Climate Computing Centre (DKRZ) through support from the Bundesministerium für Bildung und Forschung (BMBF). We thank A. Pfeiffer from DLR for the internal review and helpful comments.

Appendix: Calculation of AHEAD parameters for the Schmidt-Appleman criterion

Table 6 shows the aircraft parameters used to calculate the slope G in equation (4.1), i.e. to calculate the specific heat content of the combined fuel use Q, the emission index of water vapour EI_{H_2O}, and the overall propulsion efficiency η, via the equations (see also Table 7):

$$EI^X_{H_2O} = \frac{\dot{m}^X_{H_2O}}{\dot{m}^X_X + \dot{m}^X_{ker}} \tag{6.1}$$

$$Q^X = \frac{Q^X\,\dot{m}^X_X + Q^{ker}\,\dot{m}^X_{ker}}{\dot{m}^X_X + \dot{m}^X_{ker}} \tag{6.2}$$

$$\eta^X = \frac{F\,v}{(\dot{m}^X_X + \dot{m}^X_{ker})\,Q^X}, \tag{6.3}$$

where X denotes the values for the specific fuel, either LH2 or LNG and $v = 250\,\mathrm{m\,s^{-1}}$ the speed of the aircraft.

Table 6: Input parameters for the calculation of the Schmidt-Appleman criterion for the AHEAD aircraft. The superscript X refers to either LH2 or LNG.

Parameter	Symbol	Unit	AHEAD	
			LH2	LNG
Net. Thrust	F	kN	52.93	53.91
Fuel flow kerosene	$\dot{m}^X_{ker}$	$\mathrm{kg\,s^{-1}}$	0.08	0.07
2nd fuel flow	$\dot{m}^X_X$	$\mathrm{kg\,s^{-1}}$	0.25	0.62
H_2O emission rate	$\dot{m}^X_{H_2O}$	$\mathrm{kg\,s^{-1}}$	2.38	1.48

Table 7: Calculated parameters for the Schmidt-Appleman criterion of the AHEAD aircraft.

Parameter	Symbol	Unit	AHEAD		Conv.
			LH2	LNG	
H_2O-Emission Index	EI_{H_2O}	$kg\,kg^{-1}$	7.21	2.15	1.25
Specific heat content	Q	$MJ\,kg^{-1}$	101	49.3	43.2
Overall propulsion efficiency	η	–	0.40	0.40	0.33
Slope at FL 430	G	$Pa\,K^{-1}$	3.1	1.9	1.1

References

Appleman, H, 1953: The formation of exhaust condensation trails by jet aircraft. – Bull. Amer. Meteor. Soc. **34**, 14–20.

Bock, L., 2014: Modellierung von Kondensstreifenzirren: Mikrophysikalische und optische Eigenschaften. – Dissertation, Ludwig-Maximilians-Universität München, pp. 105, published online: http://edoc.ub.uni-muenchen.de/17026/1/Bock_Lisa.pdf.

Bock, L., U. Burkhardt, 2016: The temporal evolution of a long-lived contrail cirrus cluster: Simulations with a global climate model. – J. Geophys. Res., **121**, 3548–3565, DOI: 10.1002/2015JD024475.

Burkhardt, U., B. Kärcher, 2009: Process-based simulation of contrail cirrus in a global climate model. – J. Geophys. Res. **114**, D16201, DOI: 10.1029/2008JD011491.

Burkhardt, U., B. Kärcher, 2011: Global radiative forcing from contrail cirrus. – Nat. Climate Change **1**, 54–58, DOI: 10.1038/nclimate1068.

Burkhardt, U., B. Kärcher, M. Ponater, K. Gierens, A. Gettleman, 2008: Contrail cirrus supporting areas in model and observations. – Geophys. Res. Lett. **35**, L16808. DOI: 10.1029/2008GL034056.

Dahlmann, K., V. Grewe, C. Frömming, U. Burkhardt, 2016: Can we reliably assess climate mitigation options for air traffic scenarios despite large uncertainties in atmospheric processes? – Transport. Res. D., **46**, 40–55.

European Commission, Communication COM, 2011: 144 final White Paper – Roadmap to a Single European Transport Area – Towards a competitive and resource efficient transport system. – Brussels.

European Commission, 2001: Flightpath 2050 Europe's Vision for Aviation Report of the High-Level Group on Aviation Research, 32 pp., DOI: 10.2777/50266.

Eyers, C.J., P. Norman, J. Middel, M. Plohr, S. Michot, K. Atkinson, R.A. Christou, 2004: AERO2k global aviation emissions inventories for 2002 and 2025. – Tech. Rep. QINETIC/04/01113, QinetiQ Ltd., Farnborough, U.K.

Frömming, C., M. Ponater, K. Dahlmann, V. Grewe, P.D.S. Lee, R. Sausen, 2012: Aviation-induced radiative forcing and surface temperature change in dependency of the emission altitude. – J. Geophys. Res. **117**, D19, DOI: 10.1029/2012JD018204.

Grewe, V., K. Dahlmann, 2015: How ambiguous are climate metrics? And are we prepared to assess and compare the climate impact of new air traffic technologies? – Atmos. Environ. **106**, 373–374, DOI: 10.1016/j.atmosenv.2015.02.039.

Grewe, V., A. Stenke, 2008: AirClim: An efficient tool for climate evaluation of aircraft technology. – Atmos. Chem. Phys. **8**, 4621–4639, DOI: 10.5194/acp-8-4621-2008.

Grewe, V., A. Stenke, M. Ponater, R. Sausen, G. Pitari, D. Iachetti, H. Rogers, O. Dessens, J. Pyle, I.S.A. Isaksen, L. Gulstad, O.A. Søvde, C. Marizy, E. Pascuillo, 2007: Climate impact of supersonic air traffic: an approach to optimize a potential future supersonic fleet - results from the EU-project SCENIC. – Atmos. Chem. Phys. **7**, 5129–5145.

Grewe, V., M. Plohr, G. Cerino, M. Di Muzio, Y. Deremaux, M. Galerneau, P. de Saint Martin, T. Chaika, A. Hasselrot, U. Tengzelius, V.D. Korovkin, 2010: Estimates of the Climate Impact of Future Small-Scale Supersonic Transport Aircraft – Results from the HISAC EU-Project. – Aeronautical J. **114**, 199–206.

Hansen, J., M. Sato, R. Ruedy, 1997: Radiative forcing and climate response. – J. Geophys. Res. **102**, 6831–6864.

Huebsch, W., D. Lewellen, 2006: Sensitivity Study on Contrail Evolution. – 36th AIAA Fluid Dynamics Conference and Exhibit, AIAA 2006-3749, 1–14.

International Air Transport Association (IATA), 2013: IATA Technology Roadmap 4th edition. – http://www.iata.org/whatwedo/environment/Documents/technology-roadmap-2013.pdf.

Kärcher, B., F. Yu, 2009: Role of aircraft soot emissions in contrail formation. – Geophys. Res. Lett. **36**, L01804, DOI: 10.1029/2008GL036649.

Kärcher, B., U. Burkhardt, A. Bier, L. Bock, I.J. Ford, 2015: The microphysical pathway to contrail formation. – J. Geophys. Res. Atmos. **120**, 7893–7927, DOI: 10.1002/2015JD023491.

Kee, R.J., F.M. Rupley, J.A. Miller, M.E. Coltrin, J.F. Grcar, E. Meeks, H.K. Moffat, A.E. Lutz, G. Dixon-Lewis, M.D. Smooke, J. Warnatz, G.H. Evans, R.S. Larson, R.E. Mitchell, L.R. Petzold, W.C. Reynolds, M. Caracotsios, W.E. Stewart, P. Glarborg, C. Wang, C.L. McLellan, O. Adigun, W.G. Houf, C.P. Chou, S.F. Miller, P. Ho, P.D. Young, D.J. Young, D.W. Hodgson, M.V. Petrova, K.V. Puduppakkam, 2006: CHEMKIN Release 4.1, Reaction Design. – San Diego, CA.

Lee, D.S., G. Pitari, V. Grewe, K. Gierens, J.E. Penner, A. Petzold, M.J. Prather, U. Schumann, A. Bais, T. Berntsen, D. Iachetti, L.L. Lim, R. Sausen, 2010: Transport impacts on atmosphere and climate: aviation. – Atmos. Env. **44**, 4678–4734.

Leonard, G., J. Stegmaier, 1994: Development of an Aeroderivative Gas Turbine Dry Low Emissions Combustion System. – J. Engin. Gas Turbines Power **116**, 542–546, DOI: 10.1115/1.2906853.

Levy, Y., F.C. Christo, I. Gaissinski, V. Erenburg, V. Sherbaum, 2014: Design and Performance Analysis of a Gas Turbine Flameless Combustor Using CFD Simulations. – Proceedings of ASME Turbo Expo 2014, June 16–20, 2014, Düsseldorf, Germany, ASME Paper No. GT2012-68761, 543–551, DOI: 10.1115/GT2012-68761.

Meerkötter, R., U. Schumann, D.R. Doelling, P. Minnis, T. Nakajima, Y. Tsushima, 1999: Radiative forcing by contrails. – Ann. Geophys. **17**, 1080–1094.

Prusa, J., P. Smolarkiewicz, A. Wyszogrodzki, 2008: EULAG, a computational model for multiscale flows. – Comput. Fluids **37**, 1193–1207.

Rao, A.G., F. Yin, J.P. van Buijtenen, 2014: A hybrid engine concept for multi-fuel blended wing body. – Aircraft Engin. Aerospace Technol. **86**, 483–493, DOI: 10.1108/AEAT-04-2014-0054.

Reichel, T., K. Goeckeler, C.O. Paschereit, 2015a: Investigation of Lean Premixed Swirl-Stabilized Hydrogen Burner with Axial Air Injection Using OH-PLIF Imaging. – J. Engin. Gas Turbines Power **137**, 111513, DOI: 10.1115/1.4031181.

Reichel, T.G., S. Terhaar, C.O. Paschereit, 2015b: Increasing Flashback Resistance in Lean Premixed Swirl-stabilized

Hydrogen Combustion by Axial Air Injection. GTP-14-1522. – J. Eng. Gas Turbines Power **137**, GTP-14-1522; DOI: 10.1115/1.4029119.

Roskam, J., 1997: Airplane Design: Part II. – Lawrence, Kansas: Design, Analysis and Research Corporation.

Schmidt, E., 1941: Die Entstehung von Eisnebel aus den Auspuffgasen von Flugmotoren. – Schriften der Deutschen Akademie der Luftfahrtforschung **44**, 1–15.

Schumann, U., 1996: On Conditions for Contrail Formation from Aircraft Exhausts. – Meteorol. Z. **5**, 4–23.

Sölch, I., B. Kärcher, 2010: A large-eddy model for cirrus clouds with explicit aerosol and ice microphysics and Lagrangian ice particle tracking. – Quart. J. Roy. Meteor. Soc. **136**, 2074–2093.

Unterstrasser, S., 2014: Large-eddy simulation study of contrail microphysics and geometry during the vortex phase and consequences on contrail-to-cirrus transition. – J. Geophys. Res. **119**, 7537–7555, DOI: 10.1002/2013JD021418.

Unterstrasser, S., K. Gierens, 2010: Numerical simulations of contrail-to-cirrus transition – part 2: Impact of initial ice crystal number, radiation, stratification, secondary nucleation and layer depth. – Atmos. Chem. Phys. **10**, 2037–2051, DOI: 10.5194/acp-10-2037-2010.

Unterstrasser, S., N. Görsch, 2014: Aircraft-type dependency of contrail evolution. – J. Geophys. Res. Atmos. **119**, published online, DOI: 10.1002/2014JD022642.

Unterstrasser, S., R. Paoli, I. Sölch, C. Kühnlein, T. Gerz, 2014: Dimension of aircraft exhaust plumes at cruise conditions: effect of wake vortices. – Atmos. Chem. Phys. **14**, 2713–2733, DOI: 10.5194/acp-14-2713-2014.

Zhang, Y., A. Macke, F. Albers, 1999: Effect of crystal size spectrum and crystal shape on stratiform cirrus radiative forcing. – Atmos. Res. **52**, 59–75, DOI: 10.1016/S0169-8095(99)00026-5.